Electron Raman scattering in a spherical quantum dot

R. Riera
Departamento de Física, Universidad de Sonora, Apartado postal 1626, 83000 Hermosillo, Sonora, Mexico

J.L. Marin
Centro de investigación en Física, Universidad de Sonora, Apartado postal 5-088, 83190 Hermosillo, Sonora, Mexico

J.M. Bergues, R. Betancourt-Riera, and M. Fernández.
Departamento de Física, Universidad de Oriente, Santiago de Cuba, 90500 CUBA.

Recibido el 7 de mayo de 1996; aceptado el 26 de noviembre de 1997

The differential-cross-section (DCS) for an electron Raman scattering (ERS) process in semiconductors quantum-dots (QD) of spherical shape is calculated for $T = 0$ K and neglecting phonon assisted transitions. Electron states are considered assuming complete confinement within the QD. We also assume a single parabolic conduction and valence bands. Two kinds of spectra are discussed: emission spectra (DCS as a function of emitted photon energy) and excitation spectra (DCS as a function of incident photon energy). In both cases we analyze DCS for different scattering configurations. We study selection rules for the processes. Singularities in the spectra are found and interpreted. The ERS here studied can be used to provide direct information about the electron band structure of the system.

Keywords: Electron Raman scattering, quantum dots

Se calcula la sección eficaz diferencial para un proceso de dispersión Raman electrónica en puntos cuánticos semiconductores de forma esférica a la temperatura de 0 K. No se considera la interacción con los fonones y se suponen además bandas parabólicas y confinamiento completo para los estados electrónicos. Se discuten los espectros de emisión y excitación y se estudian las reglas de selección para este proceso, así como su estructura. La información resultante puede ser útil para caracterizar la estructura de bandas de este sistema de baja dimensionalidad.

Descriptores: Dispersión Raman electrónica, puntos cuánticos

PACS: 68.90.+g; 78.30.-j; 78.60.Ya

1. Introduction

Many theoretical and experimental works have been devoted to the study of different properties of the nanostructured QD, quantum size effects on the exciton energy and optical absorption spectra [1–3], electronic states and optical spectra [4–7]. Raman scattering experiments are well known to provide a powerful tool for the investigation of different physical properties of semiconductor nanostructures (superlattices, quantum-wells, etc.) [8–10]. In particular, the electronic structure of semiconductor materials and nanostructures can be thoroughly investigated considering different polarizations for the incident and emitted radiation [8–11]. In connection with this kind of experiments the calculation of the differential cross section (DCS) for Raman scattering remains a rather interesting and fundamental issue to achieve a better understanding of the man-made semiconductor nanostructures characterized by their mesoscopic dimensions [12–15].

Among the various Raman scattering processes involved in this kind of research slectron Raman scattering (ERS) seems to be a useful technique providing direct information on the energy band structure and the optical properties of the investigated systems. ERS is qualitatively explained as a two-step process: in the first step the system absorbs a photon from the incident radiation and an electron-hole-pair (EHP) is created in a virtual state (after an interband electron transition); in the second step the electron and the hole move independently of each other and emit photons of secondary radiation performing intraband transitions [16]. In the final state an EHP appears in a real state of the system, which is thus left in an excited state. The DCS for ERS, in the general case, usually shows singularities related to interband and intraband transitions. This latter result strongly depends on the scattering configurations: the structure of the singularities is varied when the photon polarizations change [17]. This peculiar feature of ERS allows to determine the sub-band structure of the system by direct inspection of the singularity positions in the spectra.

For bulk semiconductors ERS has been studied in the presence of external applied magnetic and electric fields [18–21]. In the case of a quantum-well preliminary results were reported by Riera *et al.* [16]. In the other case [23], two articles about ERS in cylindrical and rectangular quantum wire (QW), were published. It is our aim to study ERS in a quantum-dot (QD) of spherical shape. The emission and excitation spectra, in these novel systems are significantly modified due to the quasi-zero-dimensional character of the elec-

tronic states. The ERS processes are determined by electronic transitions between zero-dimensional electron or hole subbands. For the sake of simplicity we assume complete electron confinement within the QD. We also consider parabolic bands in the zero temperature case and neglect all the transitions assisted by phonons. Such simplifying assumptions facilitate the calculations but still provides a clear picture of the physical situation.

2. Model and applied theory

Let us briefly describe the model and fundamental theory applied in our calculations. The QD is of radius r_0. As explained above, we consider a single conduction (valence) band, which is split into a sub-band system due to complete electron confinement within the structure. The solution of Schrödinger equation in the envelope function approximation leads to

$$\Psi_c = \chi_c u_c = \sqrt{\frac{(2n_e+1)(n_e-m_e)!}{2\pi(n_e+m_e)!}}\left[r_o J_{n_e+\frac{3}{2}}\left(\mu_{k_e}^{n_e+\frac{1}{2}}\right)\right]^{-1} \times (r)^{-\frac{1}{2}} J_{n_e+\frac{1}{2}}\left(\mu_{k_e}^{n_e+\frac{1}{2}}\frac{r}{r_o}\right)\Gamma_{n_e}^{m_e}(\theta,\varphi)\,u_c \quad (1)$$

for conduction electrons. $J_{n+\frac{1}{2}}(\mu)$ is the Bessel function of order $n+\frac{1}{2}$. $\mu_k^{n+\frac{1}{2}}$ denotes the zeros of the Bessel function: $J_{n+\frac{1}{2}}(\mu_k^{n+\frac{1}{2}}) = 0$. $\Gamma(\theta,\varphi)$ are the spherical harmonics. u_c is the Bloch function taken at $\vec{k}_0 = 0$ in the Brillouin Zone, where (by assumption) the band extrema are located. We use spherical coordinates (r,θ,φ). The complete electron confinement in the QD implies $\chi_c|_{r_0} = 0$.

The suffix e is used to denote electronic quantities. The electronic states are described by the quantum numbers: n_e, k_e, m_e. The eigenenergies are

$$E_c(n_e,k_e) = \frac{\hbar^2}{2\mu_e}\left(\frac{\mu_{k_e}^{n_e+\frac{1}{2}}}{r_0}\right)^2 \quad (2)$$

μ_e being the electron effective mass and $E = 0$ at the bottom of the bulk conduction band. For the holes the analogous quantities are obtained essentially changing suffix e by h (labeling hole quantities).

The DCS for ERS is given by [16]

$$\frac{d^2\sigma}{d\omega_s d\Omega} = \frac{V^2\omega_s^2 n(\omega_s)}{8\pi^3 c^4 n(\omega_l)} W(\omega_s,\vec{e}_s), \quad (3)$$

where V is the normalization volume, $n(\omega)$ is the refraction index as a function of the radiation frequency, ω_s and $\vec{e}_s$ is the unit polarization vector for the emitted secondary radiation. c is the light velocity and ω_l is the frequency of the incident radiation and $W(\omega_s,\vec{e}_s)$ is the transition rate calculated according to

$$W(\omega_s,\vec{e}_s) = \frac{2\pi}{\hbar}\sum_f |M_e + M_h|^2\delta(E_f - E_i), \quad (4)$$

where

$$M_j = \sum_a \frac{\langle f|H_{js}|a\rangle\langle a|H_l|i\rangle}{E_i - E_a + i\Gamma_a} + \sum_b \frac{\langle f|H_l|b\rangle\langle b|H_{js}|i\rangle}{E_i - E_b + i\Gamma_b}. \quad (5)$$

In Eq. (6) $j = e,h$ for the cases of electrons or holes, respectively, $|i\rangle$ and $|f\rangle$ denote initial and final state of the system with their corresponding energies E_i and E_f. $|a\rangle$ and $|b\rangle$ are intermediate states with energies E_a and E_b while Γ_a and Γ_b are the corresponding life-time widths.

The operator H_l is of the form

$$H_l = \frac{|e|}{\mu_0}\sqrt{\frac{2\pi\hbar}{V\omega_l}}\vec{e}_l\cdot\vec{P}, \quad \vec{P} = -i\hbar\nabla, \quad (6)$$

where μ_0 is the free electron mass. This operator describes the interaction with the incident radiation field in the dipole approximation. The interaction with the secondary radiation field is described by the operator

$$H_{js} = \frac{|e|}{\mu_j}\sqrt{\frac{2\pi\hbar}{V\omega_s}}\vec{e}_s\cdot\vec{P}, \quad j = e,h. \quad (7)$$

This operator describes the photon emission by the electron (hole) after transitions between conduction (valence) subbands of the system. In Eq. (7) the intermediate states $|a\rangle$ represent an EHP in a virtual state (after absorption of the incident photon), while the states $|b\rangle$ are related to the "interference diagrams" [16, 24]. The latter term involves a negligible contribution whenever the energy gap E_g is large enough (for instance, this is the case of GaAs, CdTe, etc.) and will not be considered in the present work.

In the initial state $|i\rangle$ we have a completely occupied valence band, unoccupied conduction band and an incident photon of energy $\hbar\omega_l$. Thus

$$E_i = \hbar\omega_l \quad . \quad (8)$$

The final state $|f\rangle$ involves an EHP in a real state and a secondary radiation emitted photon of energy $\hbar\omega_s$. Hence

$$E_f = \frac{\hbar^2}{2\mu_e}\left(\frac{\mu_{k_e}^{n_e+\frac{1}{2}}}{r_0}\right)^2 + \frac{\hbar^2}{2\mu_h}\left(\frac{\mu_{k_h}^{n_h+\frac{1}{2}}}{r_0}\right)^2 + \hbar\omega_s + E_g. \quad (9)$$

For the intermediate states $|a\rangle$ the energies E_a are easily obtained from the above discussion.

3. Differential cross section

Using the theory depicted in Sect. 2 we can obtain, after cumbersome calculations, explicit expressions for the DCS of the ERS process. We have neglected photon wavevector in comparison with electron wave vector, in our calculation. Hence, in the final state we have: $\vec{k}_e + \vec{k}_h = 0$. We just write the final results:

$$\frac{d^2\sigma}{d\omega_s d\Omega} = \sum_{j=1}^{3} \left[\frac{d^2\sigma}{d\omega_s d\Omega}\right]_j , \tag{10}$$

where $j = 1 = e_s^z$; $j = 2 = e_s^+$; $j = 3 = e_s^-$. The e vectors represent the different polarization directions, and

$$\left[\frac{d^2\sigma}{d\omega_s d\Omega}\right]_j = \frac{27}{4}\sigma_0 \left(\frac{\hbar\omega_s}{E_0^{(S)}}\right)^2 \delta_f W_j \times (\vec{e}_s.\vec{\sigma}_j)^2 , \tag{11}$$

where

$$W_j^{(S)} = \sum_{nmk_1k_2} \left\{ \left[\left| \frac{\beta_1 Y_{j1}}{g^{k_1(n)}_{k_2(n-1)} + i\delta} \right|^2 + \left| \frac{\beta_2 Y_{j2} J_{k_1(n)}}{d^{k_1(n)}_{k_2(n-1)} + i\delta'} \right|^2 \right] \times \left| \frac{X^{k_1(n)}_{k_2(n-1)}}{p^{k_1(n)}_{k_2(n-1)} + i\delta_f} \right|^2 + \left[\left| \frac{\beta_1 Y_{j3} J_{k_2(n+1)}}{g^{k_1(n)}_{k_2(n+1)} + i\delta} \right|^2 + \left| \frac{\beta_2 Y_{j4}}{d^{k_1(n)}_{k_2(n+1)} + i\delta'} \right|^2 \right] \left| \frac{X^{k_1(n)}_{k_2(n+1)}}{p^{k_1(n)}_{k_2(n+1)} + i\delta_f} \right|^2 \right\} \tag{12}$$

and

$$g^{k_1(i)}_{k_2(i)} = \frac{\hbar\omega_s}{E_0^{(S)}} + \beta_1 \left[\left(\mu_{k_1}^{i+\frac{1}{2}}\right)^2 - \left(\mu_{k_2}^{i+\frac{1}{2}}\right)^2 \right],$$

$$d^{k_1(i)}_{k_2(i)} = \frac{\hbar\omega_s}{E_0^{(S)}} + \beta_2 \left[\left(\mu_{k_2}^{i+\frac{1}{2}}\right)^2 - \left(\mu_{k_1}^{i+\frac{1}{2}}\right)^2 \right],$$

$$p^{k_1(i)}_{k_2(i)} = \frac{\hbar\omega_l - E_g - \hbar\omega_s}{E_0^{(S)}} - \beta_1 \left(\mu_{k_1}^{i+\frac{1}{2}}\right)^2 - \beta_2 \left(\mu_{k_2}^{i+\frac{1}{2}}\right)^2 ,$$

$$J_{k(i)} = \frac{J_{i-\frac{1}{2}}\left(\mu_k^{i+\frac{1}{2}}\right)}{J_{i+\frac{3}{2}}\left(\mu_k^{i+\frac{1}{2}}\right)},$$

$$X^{k_1(i)}_{k_2(i)} = \frac{\mu_{k_1}^{i+\frac{1}{2}} \mu_{k_2}^{i+\frac{1}{2}}}{\left(\mu_{k_1}^{i+\frac{1}{2}}\right)^2 - \left(\mu_{k_2}^{i+\frac{1}{2}}\right)^2}. \tag{13}$$

The $Y_{j\alpha}$ terms are only characterization coefficients of the DCS of each polarization

$$Y_{11} = \sqrt{2}q\frac{a!}{b!}b = Y_{12}, \quad Y_{13} = \sqrt{2}q\frac{a!}{b!}(a+1) = Y_{14},$$

$$Y_{21} = q\frac{a!}{b!} = Y_{32}, \quad Y_{22} = -q\frac{a!}{b!}b(b-1) = Y_{31}, \tag{14}$$

$$Y_{23} = -q\frac{a!}{b!} = Y_{34}, \quad Y_{24} = q\frac{a!}{b!}(a+2)(a+1) = Y_{33}.$$

We have

$$\sigma_0 = \frac{4\sqrt{2}Ve^4 \left|\vec{e}_l \cdot \vec{P}_{cv}\right|^2 n(\omega_s)\mu_r^{1/2} E_0^{3/2}}{9\pi^2\mu_0^2\hbar^4 c^4 n(\omega_l)\omega_l\omega_s}, \tag{15}$$

and

$$\beta_1 = \left(1+\beta^{-1}\right)^{-1}, \quad \beta_2 = (1+\beta)^{-1}, \quad \beta = \frac{\mu_h}{\mu_e},$$

$$E_0 = \frac{\hbar^2}{2\mu_r r_0^2}, \quad \mu_r^{-1} = \mu_e^{-1} + \mu_h^{-1}. \tag{16}$$

Deduction of Eqs. (11) and (12) requires that

$$\delta(E_i - E_f) \to \frac{1}{\pi}\frac{\Gamma_f}{(E_f - E_i)^2 + \Gamma_f^2}, \tag{17}$$

assuming a finite lifetime for the EHP in the final state, while

$$\delta_f = \frac{\Gamma_f}{E_0}, \quad \delta = \frac{\Gamma_a}{E_0}, \quad \delta' = \frac{\Gamma_b}{E_0}, \tag{18}$$

and

$$\vec{\sigma}_\pm = \frac{1}{\sqrt{2}}\left(\hat{X} \pm i\hat{Y}\right). \tag{19}$$

the vectors $\hat{X}$, $\hat{Y}$ and $\hat{Z}$ are unit vectors along the corresponding Cartesian axis.

The interband matrix element of the operator $\vec{P}$ is denoted as

$$\vec{P}_{cv} = \frac{1}{V_0}\int_{V_0} u_c^* \vec{P} u_v \, d^3r, \tag{20}$$

the above matrix element is evaluated at $\vec{k}_0 = 0$ in the Brillouin Zone while V_0 is the unit cell volume.

Let us make some remarks concerning the above equations. For a general scattering configuration we should have three terms in the DCS, as explicitly seen in Eq. (10). However, for particular choice of the scattering configuration some of these terms could be absent. For instance, if we have backscattering configuration with $\hat{Z}$ parallel to the radiation wavevector $\vec{k}$, then the other configurations will not contribute to the DCS. In general for all the scattering configuration the contribution to the DCS is given by (11) and (12). In the configuration where scattered radiation wavevector is parallel to the x-axis with polarization $\vec{e}_s \parallel \hat{z}$, *i.e.*, $\bar{Z}(\vec{e}_l, \vec{e}_{sz})X$ only the first term at the right-hand-side of Eq. (10) will be present in the DCS. In these configurations the emission spectrum of ERS in a spherical QD shows maxima at the following values of ω_s:

$$\omega_s \to \omega_e(n_e; k_e, k_h) = \frac{\beta_1 E_0}{\hbar}\left[\left(\mu_{k_e}^{n_e+\frac{1}{2}}\right)^2 - \left(\mu_{k_h}^{n_h+\frac{1}{2}}\right)^2\right], \tag{21}$$

$$\omega_s \to \omega_h(n_e; k_e, k_h) = \frac{\beta_2 E_0}{\hbar}\left[\left(\mu_{k_h}^{n_h+\frac{1}{2}}\right)^2 - \left(\mu_{k_e}^{n_e+\frac{1}{2}}\right)^2\right]. \tag{22}$$

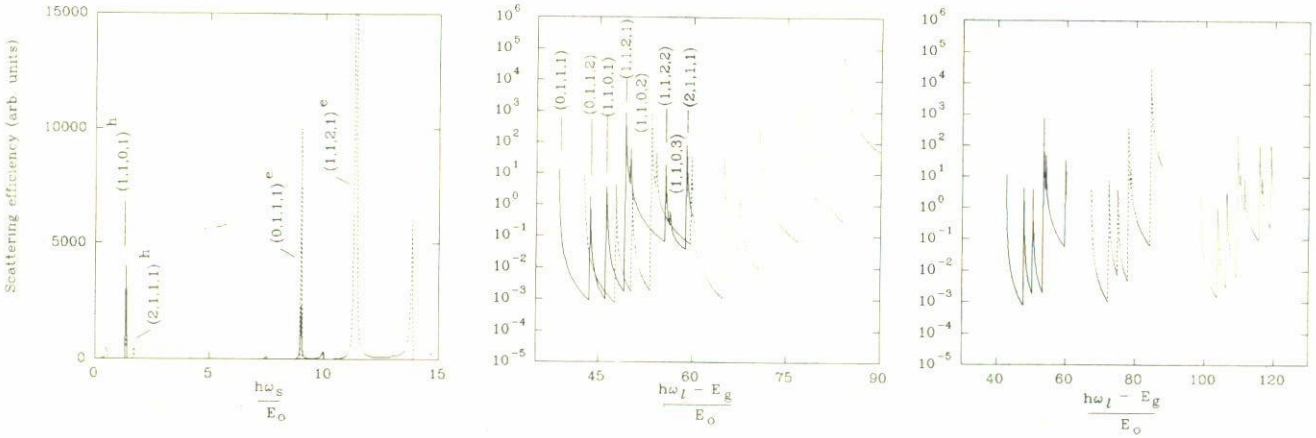

FIGURE 1. ERS cross-section (in arbitrary units of σ_0) for a GaAs spherical quantum-dots in the scattering configuration $\bar{Z}(\vec{e}_l, \hat{Z})X$. We have set: $\Gamma_f = 3$ meV and $\Gamma_a = \Gamma_b = 1$ meV. a) Scattering efficiency as a function of $\hbar\omega_s/E_0$ (emission spectrum). The solid curve correspond to $\hbar\omega_l = 2.3$ eV, the dashed curve to $\hbar\omega_l = 2.9$ eV, in both case $r_0 = 4$ nm. Resonant transitions are indicated by $\omega^e\,(n_e, k_e, n_h, k_h)$ and $\omega^h\,(n_e, k_e, n_h, k_h)$ corresponding to electron or hole intersubbands transitions [see Eqs. (21) and (22)]. b) Scattering efficiency as a function of $(\hbar\omega_l - E_g)/E_0$ (excitation spectrum). The solid curve correspond to $r_0 = 3$ nm and $\hbar\omega_s = 2$ eV, the medium dashed curve to $\hbar\omega_s = 2.3$ eV and the short dashed curve correspond to $r_0 = 4$ nm and $\hbar\omega_s = 2$ eV. c) Scattering efficiency as a function of $(\hbar\omega_l - E_g)/E_0$ (excitation spectrum). The solid curve correspond to $r_0 = 3$ nm, the medium dashed curve to $r_0 = 4$ nm and the short dashed curve correspond to $r_0 = 5$ nm, in all cases we have chosen $\hbar\omega_s = 2.3$ eV.

As can be seen from (21) or (22) these frequencies correspond to electron transitions connecting the sub-band edges for a process involving just the conduction or just the valence band (*i.e.*, intraband transitions). The following selection rule is fulfilled: $n_h = n_e \pm 1$; the minus sign applies to (21) and the plus sign to (22).

Other singularities of Eqs. (11) and (12) occur whenever $p = 0$. Such singularities are mainly related to certain values of the frequency ω_l of the incident photon. For the excitation spectra the positions of these singularities are given as follows:

$$\omega(n_e; k_e, k_h) = \frac{1}{E_0}(\hbar\omega_l - E_g) = \frac{\hbar\omega_s}{E_0} + \beta_1 \left(\mu_{k_e}^{n_e+\frac{1}{2}}\right)^2 + \beta_2 \left(\mu_{k_h}^{n_h+\frac{1}{2}}\right)^2 . \quad (23)$$

Here the selection rule $n_h = n_e \pm 1$ must be fulfilled. The peaks related to the latter singularities correspond to interband EHP transitions and their positions depend on the incident radiation frequency ω_l for both excitation and emission spectra. The singularities involved in Eqs. (21) and (22) are independent of ω_l and correspond to intraband transitions. These kind of singularities are present in the emission spectra only.

4. Discussion and conclusions

As discussed in Sect. 3, we have computed the emission and excitation spectra of the ERS process for a given polarization $\vec{e}_{sz}$ of the emitted radiation. The physical parameters entering in our formulas were taken for the GaAs case; *i.e.*, $E_g = 1.43$ eV; $\mu_e = 0.0665\mu_0$; $\mu_h = 0.45\mu_0$ (the heavy hole band).

Figure 1a shows the so-called "Emission Spectra" in which we have plotted,

$$\frac{1}{\sigma_0}\left[\frac{d^2\sigma}{d\omega_s d\Omega}\right] \quad vs. \quad \hbar\omega_s/E_0,$$

for the spherical QD.

Figures 1b and 1c show the so-called "Excitation Spectra", in which we plotted,

$$\frac{1}{\sigma_0}\left[\frac{d^2\sigma}{d\omega_s d\Omega}\right] \quad vs. \quad \frac{1}{E_0}(\hbar\omega_l - E_g),$$

for the spherical QD. The quantity $1/\sigma_0\left[d^2\sigma/d\omega_s d\Omega\right]$ is frequently called "Scattering Efficiency" (S.E).

The excitation spectrum for the spherical QD, was computed for the scattering configuration $\bar{Z}(\vec{e}_l, \hat{Z})X$. In this case only the first term at the right-hand side of (10) contributes, thus, we do not have any singularities, that is, for the fixed values $\hbar\omega_s$ and r_0 the expressions (21) and (22) do not contribute. Furthermore, for certain values of ω_l we can find abrupt changes in the curve slope which correspond to different thresholds related to the points where a given subband begin to contribute to the DCS. This explain the step-like character of the curve. The lowest admissible value of $\hbar\omega_l - E_g$ is defined by the minimum value of $\mu_k^{n+\frac{1}{2}}$. For higher values of $\hbar\omega_l - E_g$ new sub-bands begin to contribute, thus defining the other thresholds seen in the figures. We give explicit indication of the points where the thresholds are present, specifying

the involved sub-bands. Figure 1a shows the emission spectrum for the same scattering configuration. The incident radiation frequency was fixed as $\hbar\omega_l = 2.3$ eV and $\hbar\omega_l = 2.9$ eV. We can observe abrupt changes in the slope, thus providing a certain step-like dependence of the S.E. The points where the curve slope presents abrupt changes are related to threshold values of $\hbar\omega_s$ representing the incorporation of new sub-bands to the process. It should be realized that, for lower values of $\hbar\omega_s$, more sub-bands can participate in the emission process. The condition $\hbar\omega_l - \hbar\omega_s - E_g > E_0 \left(\mu_k^{n+\frac{1}{2}}\right)^2$ must be fulfilled in order to have the emission of secondary radiation photons. For fixed values of $\hbar\omega_l$, E_g, and E_0, the threshold positions are defined by $\mu_k^{n+\frac{1}{2}}$. This is explicitly indicated in Fig. 1b.

In Fig. 1a we show the emission spectra for the $\bar{Z}(\vec{e}_l, \hat{Z})X$ configuration for the QD. We have chosen $r_0 = 4\,\text{nm}$. It can be observed that for $\hbar\omega_l = 2.3$ eV the differential cross section display only two singularities at $\omega^e\,(0,1,1,1)$, and $\omega^h\,(1,1,0,1)$, while for $\hbar\omega_l = 2.9$ eV four singularities are observe at $\omega^e\,(0,1,1,1)$, $\omega^h\,(1,1,0,1)$, $\omega^e\,(1,1,2,1)$, and $\omega^h\,(2,1,1,1)$. We should note that the ω_s values for which we find singularities do not depend on the incident radiation frequency ω_l and only depend on the energy differences between the valence and conduction subbands for the fixed value r_0. For higher energies $\hbar\omega_l$ of the incident radiation photon we shall observe a large number of singular peaks in the emission spectra as can be deduced from (21) and (22). For fixed value of ω_l we can also observe a certain step-like behavior at give values of ω_s. The maximum number of steps is determined by (23). The position of the steps in the spectra depend on the value chosen for ω_l.

In Fig. 1b we show the excitation spectra for a QD for the same scattering configuration as in Fig. 1a. In the case, $\hbar\omega_s$ is fixed and $\hbar\omega_l$ is a variable quantity. The other parameters coincide with those of Fig. 1a. We observe the same behavior in the spectra for different values of r_0 with the same $\hbar\omega_s$ as those different values of $\hbar\omega_s$. The resonant transitions are indicated only in one curve, because they are same in all curve only we should keep the same order, which is given by expression (23). We also observe a threshold for the lower values of $(\hbar\omega_l - E_g)\,E_0^{-1}$ when $\mu_{k_e}^{n_e+\frac{1}{2}}$ and $\mu_{k_h}^{n_h+\frac{1}{2}}$ take their minimum values for fixed values of $\hbar\omega_s$ and r_0.

In Fig. 1c we show the excitation spectra for QD for three values of r_0, but we have now chosen $\hbar\omega_s = 2.3$ eV in all cases. In this graph, only a shift in the spectra can be observed.

In the present work we have applied a simplified model for the electronic structure of the system. In a more realistic case we should consider coupled band structure using a calculation model like that of Luttinger-Kohn or the Kane model. We also assumed an infinite potential barrier for the electron at the QD interface. A calculation assuming a finite barrier would be better, but it is also possible to introduce a certain redefined effective mass for the infinite-barrier case leading to the correct energy levels for electrons and holes (see for instance Ref. 25). The above mentioned assumptions would lead to better results but entail more complicated calculations. However, within the limits of our simple model we are able to account for the essential physical properties of the discussed problem. The fundamental features of the DCS, as described in our paper, should not change very much in the real QD case. It can be easily proved that the singular peaks in the DCS will be present irrespective of the model used for the subband structure and may be determined for the values of $\hbar\omega_s$ equal to the energy difference between two subbands: $\hbar\omega_s^{e(h)} = E_\alpha^{e(h)} - E_\beta^{e(h)}$, where $E_\alpha^{e(h)} > E_\beta^{e(h)}$ are the respective electron (hole) energies in the subbands. Similarly, we shall have a step-like dependence in the DCS for $\hbar\omega_l = \hbar\omega_s + E_g + E_\alpha + E_\beta$. Up to the present there is a lack of experimental work for this type of ERS. The major interest of our calculations is to stimulate experimental research in this direction.

1. Y. Wang and N. Herron, *J. Phys. Chem.* **95**, (1991) 525.
2. Y. Wang and N. Herron, *Phys. Rev. B* **42**, (1990) 7253.
3. R. Ramirez *et al.*, *J. Appl. Phys.* **77** (10) (1995).
4. V. Halonen, T. Chaxraborty, and P. Pietiläinen, *Phys. Rev. B* **45** (1992) 5980.
5. M. Sawamura and W. Ermler, *J. Phys. Chem.* **94** (1994) 7805.
6. J.L. Marín, R. Rosas, and A. Uribe, *Am. J. Phys.* **63** (1995) 460.
7. W. Que, *Phys. Rev. B* **45** (1992) 11036.
8. M. Cardona and G. Güntherodt, (editors) "Light Scattering in Solids V," Vol. 66 in *Topics in Applied Physics*, (Heidelberg, Springer, 1989).
9. M. Cardona, *Superlattices and Microstructures* **7** (1990) 183.
10. M.V. Klein, *IEEE Journal of Quantum Electronics* **QE-22**, (1986) 1760.
11. A. Pinczuk and E. Burstein, in "Light Scattering in Solids I," Vol. 8 of *Topics of Applied Physics*, edited by M. Cardona, (Heidelberg, Springer, 1983).
12. C. Colvard *et al.*, *Phys. Rev. B* **31** (1985) 2080.
13. A. Cros, A. Cantarero, C. Trallero-Giner, and M. Cardona, *Phys. Rev. B* **46** (1992) 12627.
14. A.J. Shields *et al.*, *Phys. Rev. B* **46** (1992) 6990.
15. A.K. Sood, J. Menéndez, M. Cardona, and K. Ploog, *Phys. Rev. Lett.* **54** (1985) 2111.
16. R. Riera, F. Comas, C. Trallero-Giner, and S.T. Pavlov, *Physica Status Solidi* (b) **148** (1988) 533.
17. M. Cardona and G. Güntherodt, (editors) "Light Scattering in Solids II," Vol. 50 in *Topics in applied Physics*, (Berlin, Springer, 1982).

18. F. Bechstedt, R. Enderlein, and K. Peuker, *Physica Status Solidi* (b) **68** (1975) 43.

19. F. Comas, C. Trallero-Giner, I.G. Lang, and S.T. Pavlov, *Fiz. Tverdovo Tela* **27**, (*Soviet Physics Solid State* **27** 32) (1985) 57.

20. A.V. Goltzev, I.G. Lang, and S.T. Pavlov, *Physica Status Solidi* (b) **94** (1979) 37.

21. R.F. Wallis and D.L. Mills, *Phys. Rev. B* **2** (1970) 3312.

22. J.M. Bergues, R. Riera, C. Trallero-Giner, and F. Comas, *J. Phys. Condens Matter.* **7** (1995) 7273.

23. J.M. Bergues, A. Villares-Ferrer, and R. Riera, submitted to *Physica Status Solidi* (b) (1995).

24. F. Comas, C. Trallero-Giner and R. Pérez-Alvarez, *J. of Physics C* **19** (1986) 6479.

25. C. Trallero-Giner and J. López-Gondar, *Physica B* **138** (1986) 287.